

# Effect of deposition rate on microstructure and mechanical properties of wire arc additive manufacturing of Ti-6Al-4V components

ZHANG Pei-lei<sup>1,2,3</sup>, JIA Zhi-yuan<sup>1,2</sup>, YAN Hua<sup>1,2</sup>, YU Zhi-shui<sup>1,2</sup>,  
WU Di<sup>1,2</sup>, SHI Hai-chuan<sup>1,2</sup>, WANG Fu-xin<sup>1,2</sup>, TIAN Ying-tao<sup>4</sup>,  
MA Song-yun<sup>5</sup>, LEI Wei-sheng<sup>1,2</sup>

1. School of Materials Engineering, Shanghai University of Engineering Science, Shanghai 201620, China;
2. Shanghai Collaborative Innovation Center of Laser Advanced Manufacturing Technology, Shanghai 201620, China;
3. Fraunhofer Institute for Laser Technology ILT, Aachen 52074, Germany;
4. Department of Engineering, Lancaster University, Lancaster LA1 4YW, United Kingdom;
5. Institute of General Mechanics, RWTH Aachen University, Aachen 52062, Germany

---

**Abstract:** Wire arc additive manufacturing (WAAM) is a novel manufacturing technique by which high strength metal components can be fabricated layer by layer using an electric arc as the heat source and metal wire as feedstock, and offers the potential to produce large dimensional structures at much higher build rate and minimum waste of raw material. In the present work, a cold metal transfer (CMT) based additive manufacturing was carried out and the effect of deposition rate on the microstructure and mechanical properties of WAAM Ti-6Al-4V components was investigated. The microstructure of WAAM components showed similar microstructural morphology in all deposition conditions. When the deposition rate increased from 1.63 to 2.23 kg/h, the ultimate tensile strength (UTS) decreased from 984.6 MPa to 899.2 MPa and the micro-hardness showed a scattered but clear decline trend.

**Keywords:** wire and arc additive manufacturing; titanium alloys; cold metal transfer; deposition rate

---

## 1 Introduction

Ti-6Al-4V titanium alloy is widely used in aviation, aerospace and other fields owing to its high specific strength, good corrosion resistance and outstanding high-temperature performance [1–4]. However, it is difficult to process by traditional machining, due to the low thermal conductivity and high chemical activity of Ti alloy, causing excessive tool wearing and difficulties in forming chips [5]. The recent emergence of additive manufacturing overcomes the limitation of machining titanium alloys and offers great potential in producing highly complex 3D structures through a layerwise approach with little waste and much shorter lead time [6–8].

Wire arc additive manufacturing (WAAM), using an electric arc as the heat source and metal wire as feedstock based on welding principles, offers the advantage of producing large dimensional structures layer by layer at a high build rate and minimum waste of raw material [9]. In the WAAM process, wire is fed at a controlled rate into an electric arc and is melted onto the substrate or the previously deposited layer, leading to a much higher deposition rate than powder-based metal additive manufacturing processes [10, 11]. It has great potential in reducing the cost of tooling, energy consumption and carbon footprint. Wire arc additive manufacturing of Ti-6Al-4V has become particularly attractive to the aerospace industry as it can significantly reduce the buy-to-fly ratio, i.e., the weight ratio between raw material and final parts, cut the cost of expensive high grade Ti alloys and overcome the difficulties in traditional machining [12–16].

Large dimensional titanium components can now be successfully fabricated by WAAM based on various welding principles, such as gas metal arc welding (GMAW) [12, 17], gas tungsten arc welding (GTAW) [18, 19], and plasma arc welding (PAW) [20, 21]. Typically, the macrostructure of WAAM deposited Ti-6Al-4V, no

---

matter what type of WAAM is performed, is featured by epitaxial growth of large columnar prior- $\beta$  grains across multiple layers [19, 22]. The deposited material undergoes a melting and solidification process followed by multiple heat treatment cycles due to the continuous deposition of subsequent layers [23]. Titanium has a hexagonal close-packed crystalline structure, called the alpha ( $\alpha$ ) phase, and transforms into a body-centered cubic structure, called the beta ( $\beta$ ) phase, at a temperature above 883 °C. During the WAAM process, solidified material may experience the “ $\beta \rightarrow \alpha$ ” phase transformation several times and end up with a fine  $\alpha$ -lath and a small amount of residual  $\beta$  phase. Besides, the repeated thermal impact can lead to inhomogeneity in the local alloy composition [24]. WAAM structure often has a high level of residual stress and anisotropic mechanical properties [8, 15, 25, 26]. Through the efforts of the researchers, some solutions have been found to solve the poor mechanical properties of parts produced via WAAM, such as interpass mechanical rolling [26–29] and forced interpass cooling [30]. In this way, the columnar structure and residual stress can be well solved, and several studies have demonstrated promising results. At present, the mechanical properties of Ti-6Al-4V components fabricated by the WAAM process are competitive with those fabricated by conventional forging [31–33].

Compared to powder-based additive manufacturing techniques, the main advantages of wire-based techniques are the high deposition rates, the flexibility of producing large dimensional components, much easier and safer handling of the wire feedstock, and lower raw material costs [34, 35]. However, the excessive heat input brought by the large deposition rate accumulated throughout the WAAM process has a significant impact on the microstructure and mechanical properties in the final component. In a study carried out by WU et al [36], the heat accumulation during the GTAW-WAAM process causes variation of the microstructure and mechanical properties along the build direction. The microstructure of thin-walled parts at different locations presented different characteristics due to different heat dissipation conditions. Among them, in the middle of the deposited thin-walled part feature, due to a large amount of heat accumulation, the microstructure in the solidified metal has a fully lamellar  $\alpha$  morphology and interwoven with basketweave structures. Although the heat input and thermal cycles are critical factors in determining the quality of the WAAM components, the influence of heat accumulation on the microstructure and final mechanical properties is still not fully understood and a quantitative correlation between these two is still yet to be established. For a certain WAAM process, because the deposition rate (DR) is physically controllable during the process, it can be directly linked with the heat input and therefore can be used as a controlling factor for quantitative study.

TIAN et al [37] analyzed the changes of the titanium/copper interface under different CMT arc modes. GOU et al [38] used CMT arc to perform arc additive manufacturing of Ti-6Al-4V, and conducted heat treatment and mechanical property testing on the formed parts. CMT is a variant GMAW based on a controlled dip transfer mechanism that offers low heat input, almost zero spatter and high process tolerance. Because CMT arc as a heat source has the above advantages of arc additive manufacturing, CMT arc is widely used in aviation and aerospace, automobiles and bridges.

In this study, the influence of DR on the microstructure and mechanical properties of Ti-6Al-4V components produced by cold metal transfer (CMT) based WAAM will be systematically investigated. Ti-6Al-4V parts will be produced at different deposition rates and a correlation between CMT deposition rate and microstructure evolution and mechanical properties of the Ti-6Al-4V part will be established. It is hoped that this study can provide practical guidance for producing high quality Ti-6Al-4V components by WAAM.

## 2 Experimental

WAAM experiments were carried out using a CMT Advanced 4000R NC welding system (Fronius International GmbH, Germany) with a VR 7000-CMT 4R/G/W/F++ wire feeder. The CMT torch was mounted on an ABB IRB4600 robot arm to enable 3-dimensional movement and deposition (Figure 1(a)). Ti-6Al-4V filler wire with a diameter of 1.2 mm was used and the chemical composition is shown in Table 1. The  $\beta$  transus temperature for this composition is (996±14) °C. Because titanium is prone to absorb oxygen and nitrogen causing undesired interstitial hardening, an Ar shielding chamber was designed to protect the melt pool and heat affected zone, as shown in Figure 1(b). The specimens were built on a substrate at dimensions

of 200 mm×100 mm×5 mm with a composition as the same as the filler wire.

Three specimens in a single pass wall geometry were built layer by layer at different DR through a uni-directional deposition at the  $X$ - $Y$  plane. The layer thickness ( $\Delta Z$ ) of all specimens was set at 3.8 mm and the interpass temperature was 100 °C. The length of all specimens was 90 mm while the width and

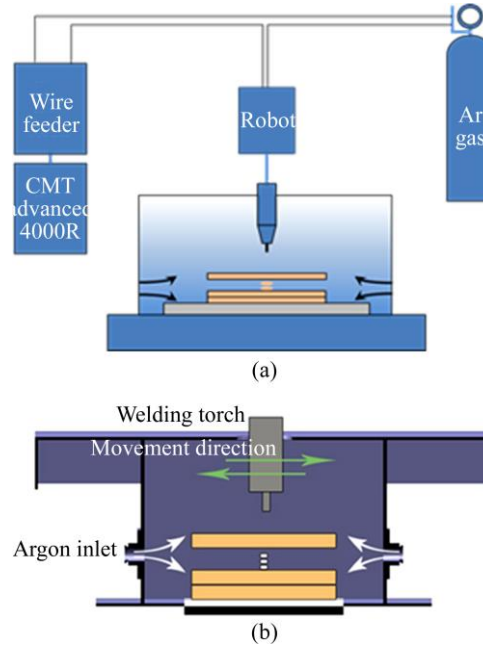


**Figure 1** CMT WAAM system: (a) Robot system; (b) Ar shielding chamber

height varied, as shown in Table 2. The DR was calculated by the mass of the as-built components divided by the deposition time. The density of Ti-6Al-4V was 4450 kg/m<sup>3</sup>. The Ar flow rate was 2 L/min in the shielding chamber and 20 L/min co-axially along with the torch. The parameters of the experimental setting are listed in Table 2. The wire feeding speeds were 5.4, 6.4 and 7.4 m/min and the DRs were 1.63, 1.93 and 2.23 kg/h correspondingly, i.e., an increase of 18.4% and 36.8% in samples 2 and 3, respectively.

After WAAM deposition, electrical discharge machining (EDM) was employed to cut tensile specimens and metallographic samples. The cross-sectional surface was then ground and polished

**Table 1** Chemical composition of Ti-6Al-4V substrate and Ti-6Al-4V welding wire (wt.%)

Alloy	w(Al)/%	w(V)/%	w(C)/%	w(Fe)/%	w(H)/%	w(N)/%	w(O)/%	Ti
Ti-6Al-4V substrates	6.20	4.0	0.08	0.40	0.015	0.05	0.20	Balanced
Ti-6Al-4V wire	6.10	4.0	0.08	0.30	0.015	0.03	0.20	Balanced

**Table 2** WAAM parameters for Ti-6Al-4V and geometries of specimens

Sample No.	Travel speed (TS)/(m·min <sup>-1</sup> )	Wire feed speed/(m·min <sup>-1</sup> )	$U$ (average voltage)/V	$I$ (average current)/A	Deposition rate/(kg·h <sup>-1</sup> )	Width/mm	Height/mm	Length/mm
1	0.252	5.4	11.8	92	1.63	4.5	31	90
2	0.252	6.4	12.2	105	1.93	5.1	33	90
3	0.252	7.4	12.3	108	2.23	5.8	35	90

and etched with Kroll's reagent for taking macro-scale morphology by optical microscope. An S-3400N scanning electron microscope (SEM) was used to observe the microstructure of the cross section at the  $Y$ - $Z$  plane and the fracture morphology of the tensile specimen. Energy dispersive X-ray analysis (EDAX) was carried out to analyze the chemical content and element distribution. The location and dimension of the tensile test specimens are illustrated in Figure 2 by following ASTM E8 2016 standard. Tensile tests were carried out by using an HB series 250 kN electro-hydraulic servo fatigue material testing machine manufactured by

Zwick/Roell, Germany. In addition, microhardness mapping was performed on the Y-Z plane along the building direction by using an HXD-1000TMC microhardness tester.

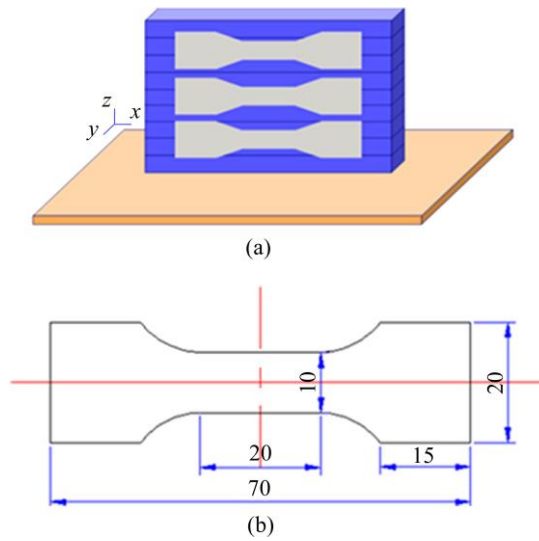


**Figure 2** Tensile sample dimension and sampling positions: (a) Sampling position; (b) Tensile specimen dimension (Unit: mm)

### 3 Results and discussion

#### 3.1 Microstructure

The morphologies of the parts produced at three different wire feed speeds are similar, so the most representative sample 2 was used here for the analysis of the morphology. The single pass wall structures were successfully built with the parameters listed in Table 2. Figure 3(a) shows the morphology of sample 2, the surface of which was slightly oxidized, indicating the argon shielding still needs some improvement (Sample 3 also has slight oxidation). The overview of the horizontal deposition layers can be seen in Figure 3(b). Large coarse columnar prior  $\beta$  grain structure can be seen growing through multiple layers, which are typical in WAAM deposition of titanium alloys due to the relatively small cooling rate and unidirectional thermal dissipation. Regularly spaced dark/bright heat affected zone (HAZ) banding with a slight offset from the deposition interlayer boundaries can also be observed on etched cross-section, as shown in Figure 3(c), except in the last few deposition layers.

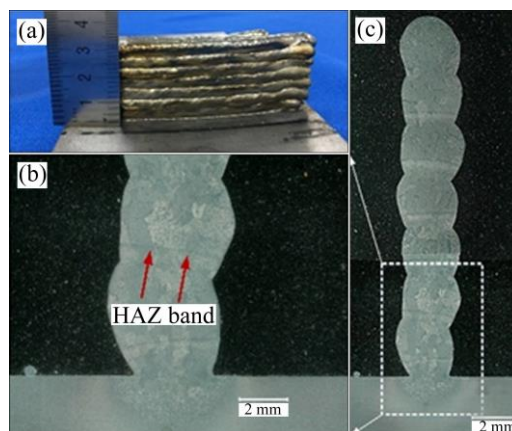


**Figure 3** Morphology of sample 2 deposited by WAAM: (a) Thin wall structure; (b) Cross-section of thin-walled parts; (c) HAZ banding

Based on the phase-transformation characteristics of the Ti-6Al-4V alloy, it can be seen that the aforementioned coarse columnar prior  $\beta$  grain strips are mainly derived from the epitaxial growth of  $\beta$ -phase

from the fusion boundary. As the heat source moves forward, the high-temperature  $\beta$  phase is cooled and thereafter transformed into a mixed microstructure of  $\alpha+\beta$ , which mainly consists of Widmanstatten colony and basketweave  $\alpha$ -lamella inseted with a small portion of retaining  $\beta$  phase. Figure 4 shows the microstructure in the last deposited layers region of sample 2. The boundary of the parent  $\beta$  grain can be clearly spotted, as indicated by the area 3. Within the parent  $\beta$  grain, a basketweave structure dominates (area 4), which consists of a majority of acicular  $\alpha$  lamellar (area 1) and a small portion of retaining  $\beta$  phase, while acicular  $\alpha'$  occurs adjacent to the parent  $\beta$  grain boundary (area 3).

$$\frac{2\pi(T-T_0)kR}{Q} = \exp\frac{-v(R-x)}{2\alpha} \quad (1)$$

where  $T$  is the liquid line;  $T_0$  is the temperature of the substrate or prior deposited layer;  $v$  is the travel speed;  $k$  is the thermal conductivity;  $R$  is the radius of  $T$ ;  $Q$  is the heat input;  $x$  is the reference point; and  $\alpha$  is the thermal diffusivity rate. It is assumed that the value of  $R$  is equal to  $x$  and  $z$ , in order to calculate the  $z$  value of the cooling rate. The cooling rate is calculated by

$$\left(\frac{\partial T}{\partial t}\right)_z = \left(\frac{\partial T}{\partial t}\right)_t \left(\frac{\partial T}{\partial t}\right)_z = -2\pi kv \frac{(T-T_0)^2}{Q} \quad (2)$$

where  $k=0.067 \text{ J}/(\text{cm}\cdot\text{s}\cdot^\circ\text{C})$ ,  $v=0.252 \text{ m}/\text{min}$ ,  $T=996 \text{ }^\circ\text{C}$ , and  $Q=\eta IU$  ( $\eta=0.8$ ). The substrate temperature ( $T_0$ ) is assumed to be  $25 \text{ }^\circ\text{C}$ , and each layer would be deposited only if the temperature of the previous layers fell below  $T_0$  ( $100 \text{ }^\circ\text{C}$ ). An infrared thermometer was used to monitor the temperature. The results show that the cooling rates of samples 1, 2 and 3 were 163.4, 138.5 and 133.6 K/s in the top region, respectively. Figure 5 shows the macro-structures and micro-structures of the top region of the WAAM deposited Ti-6Al-4V component at different deposition rates. The SEM images were taken away from the prior  $\beta$  grain boundaries, as indicated by the red box on optical micrographs (Figure 4). As calculated above, a higher deposition rate corresponds to a lower cooling rate. In the three experiments conducted in this study, the cooling rates corresponding to 1.63, 1.93 and 2.23 kg/h DR were 163.4, 138.5 and 133.6 K/s, respectively. In theory, different cooling rates should lead to different nucleation and growth rates of  $\alpha$  lamella during the  $\beta \rightarrow \alpha$  phase transformation [39]. However, based on the SEM micrographs shown in Figure 5, no significant change can be observed in the central region of the prior  $\beta$  grains.

The three cooling rates resulted in very similar basketweave  $\alpha$  lamella morphology and therefore the impact of deposition rate on microstructure of WAAM Ti6Al4V is trivial. In other studies, where the DR was between 0.7 and 1.8 kg/h, the WAAM deposited Ti alloy also showed very similar morphologies [40–42]. However, a more quantitative study is still needed to draw a firm conclusion. ZHAO et al [43] developed an automated image quantification tool to retrieve the  $\alpha$  lath space; however, due to the limitation on resources, it was not possible to conduct such quantification in this study.

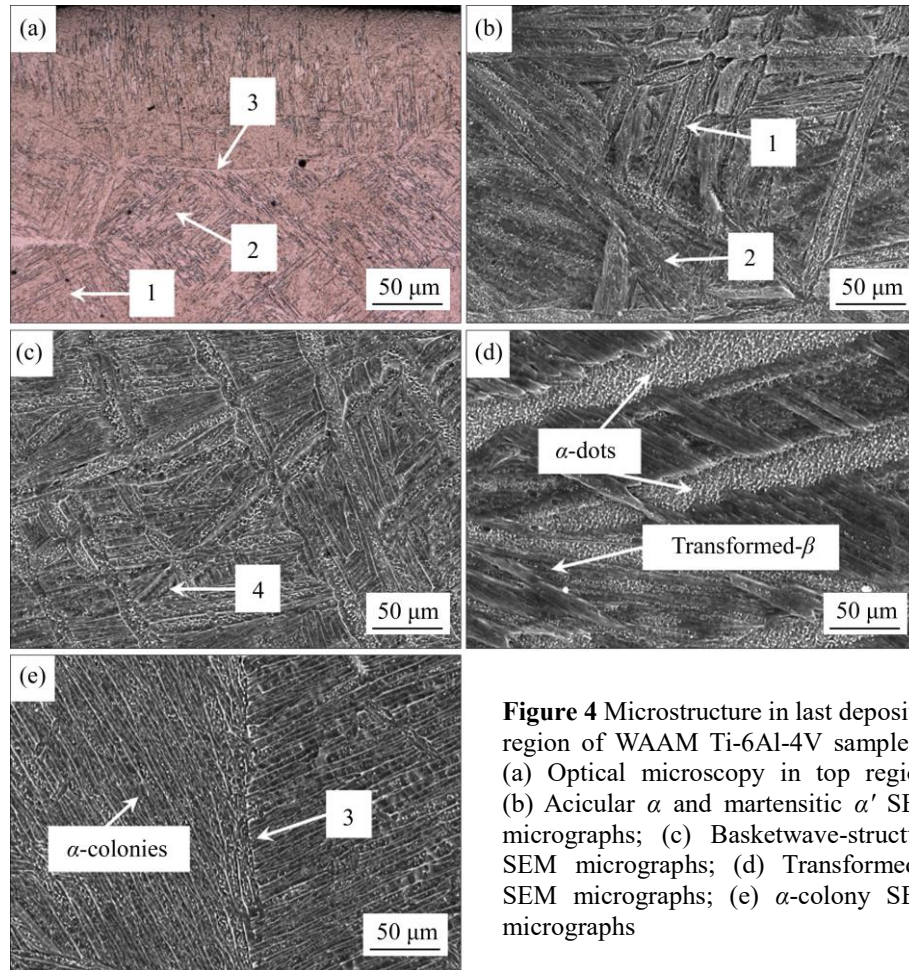


**Figure 4** Microstructure in last deposited region of WAAM Ti-6Al-4V sample 2: (a) Optical microscopy in top region; (b) Acicular  $\alpha$  and martensitic  $\alpha'$  SEM micrographs; (c) Basketwave-structure SEM micrographs; (d) Transformed- $\beta$  SEM micrographs; (e)  $\alpha$ -colony SEM micrographs

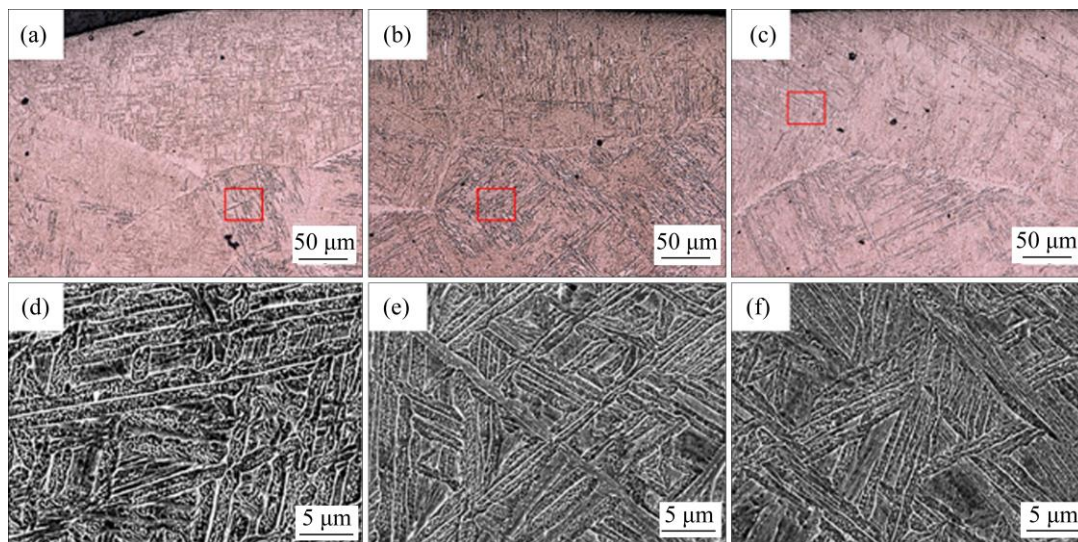


**Figure 5** Macro- and micro-structure of top region of WAAM deposited Ti6Al4V component at different deposition rates: (a, d) 1.63 kg/h; (b, e) 1.93 kg/h; (c, f) 2.23 kg/h

On the etched cross section of the WAAM deposited sample, a series of parallel HAZ bands can be observed, as shown in Figure 3. The HAZ band was caused by the successive heat treatment effect introduced by consecutive layer deposition and was firstly reported by KOBRYN and SEMIATIN [44] in laser deposition of Ti alloy. The previously laid material would be heated above the  $\beta$  transus temperature for up to 4–5 times depends on the process parameters. The sequential heat treatment leads to a change in solute partitioning in  $\alpha$  lamella and retaining  $\beta$  phase so that this chemical segregation between  $\alpha$  and  $\beta$  phases induces different

etching reaction resulting in the dark/bright HAZ band. However, such chemical variation between the phases can only possibly be revealed by high resolution TEM. Figure 6 shows the attempt of EDS measurement of the chemical composition near the HAZ band. Three small areas, as labelled as *A*, *B* and *C* in Figure 6(b), were examined in EDS, but the results showed no significant difference between them. This is due to the relatively large interaction volume of EDS indexing which cannot have enough resolution to differentiate between the fine  $\alpha$  lath and retaining the  $\beta$  phase. In the study of HO et al [24], the HAZ area was studied in detail through EDS and TEM, and it was pointed out that the cause of the HAZ area was the segregation of elements.

### 3.2 Tensile properties

Owing to the size of the WAAM Ti-6Al-4V component, off-standard tensile specimens have

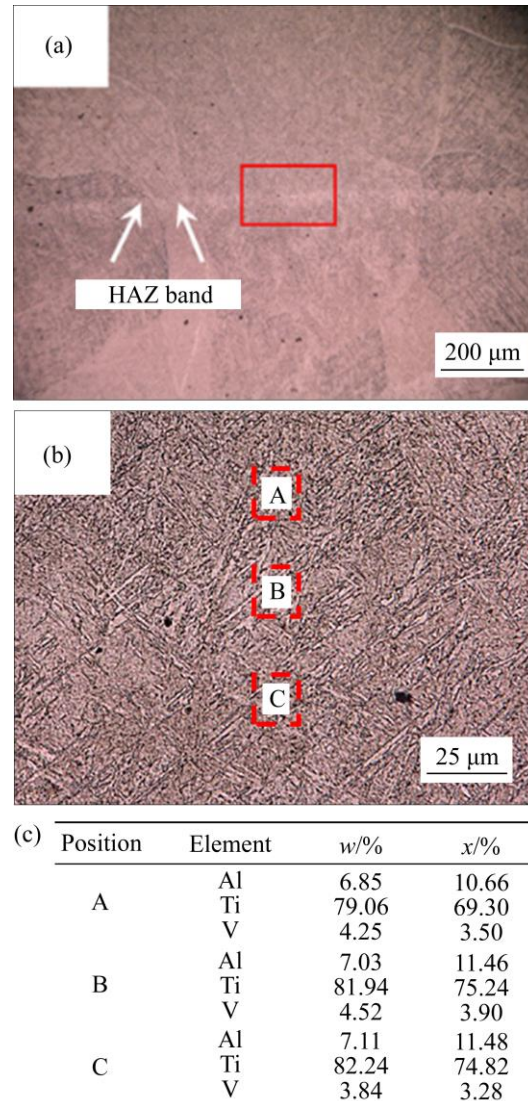


**Figure 6** EDS measurement of chemical composition near HAZ band

been extracted along the longitudinal direction, as shown in Figure 2. Three specimens were tested for each sample and the averaged results are summarized in Figure 7(d). It can be seen that the UTS values of samples 1, 2, and 3 were 984.5, 957 and 899.2 MPa, and the elongations of them were 9.48%, 7.96% and 12.62%, respectively. There is a clear trend of decrease in the UTS as the deposition rate increases, but the elongation does not follow. Figures 7(a)–(c) shows the morphology of fracture surface after tensile tests. It can be seen that all the fracture surfaces contain a large number of dimples, indicating a ductile fracture.

It can be seen from the tensile results that sample 3 has the lowest tensile strength but the highest elongation. In the process of Ti-6Al-4V parts manufactured by WAAM, the parts were subjected to several solid solution aging treatments due to the many times heat cycles. In addition, the wire feeding speed of sample

3 is the largest, and it can be seen from Table 2 that the current during the production of sample 3 is the largest, which is 108 A. This resulted in the maximum heat accumulation during the production of sample 3, and the cooling rate was reduced compared to the other two samples. In the case of long-term solution aging, the  $\alpha$  phase precipitated from the  $\beta$  phase of sample 3 is coarsened, and then uneven precipitation is formed, which increases the plasticity of sample 3 and reduces the strength [43, 44]. In addition, according to the microstructure analysis in Section 3.1, it can be seen that there is a small amount of Weinberger structure in sample 2, while the growth of Weinberger structure in sample 3 is intensified due to the extension of cooling time, thus further reducing the tensile strength of the sample [45, 46]. It should be noted that sample 2 and sample 3 had some inclusion defects, which is probably the reason for a lower elongation as the test specimen failed prematurely. Sample 2 and 3 were mentioned in Section 3.1 with slight oxidation on the surface. In the process of continuous deposition, the oxide does not overflow from the molten pool in time, thus forming impurities, which further reduces the tensile strength of the parts.

### 3.3 Micro-hardness

The micro-hardness of WAAM Ti-6Al-4V components was measured from the substrate, across the entire build, to the top region of all three samples, as shown in Figure 8(a). The hardness indent was 0.5 mm apart and the average hardness profile is plotted in Figure 8(b). For each sample, there is no obvious change of hardness from the bottom to the

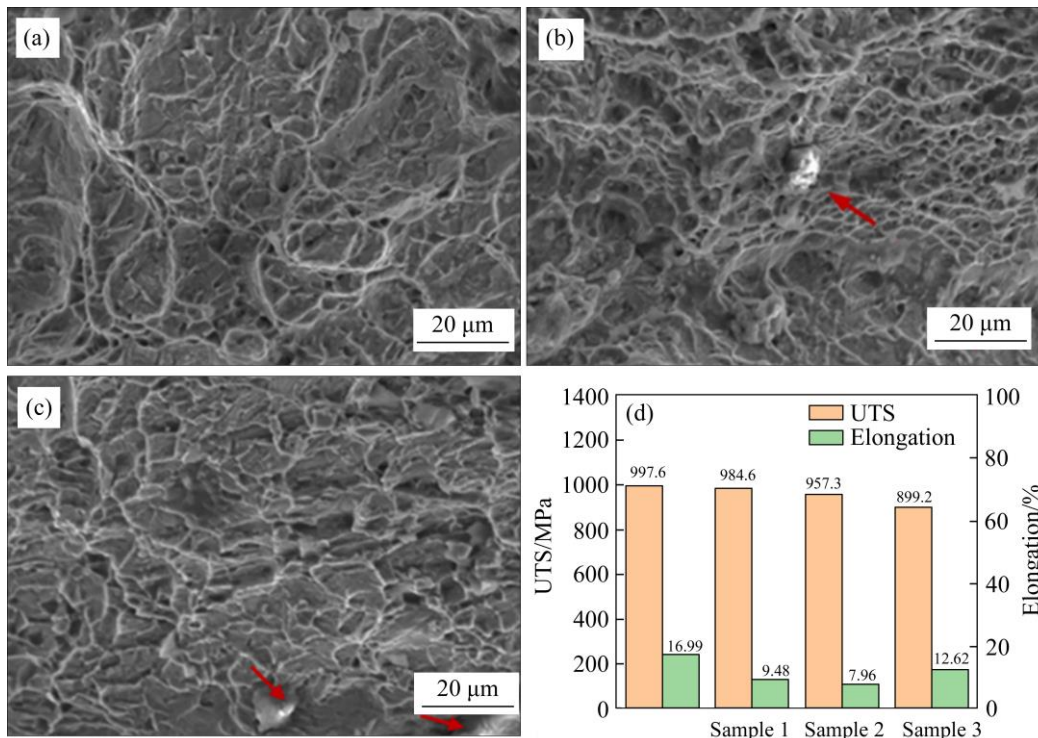


**Figure 7** Micromorphology of tensile fracture surface and tensile test results: (a) Sample 1; (b) Sample 2; (c) Sample 3; (d) Tensile test results

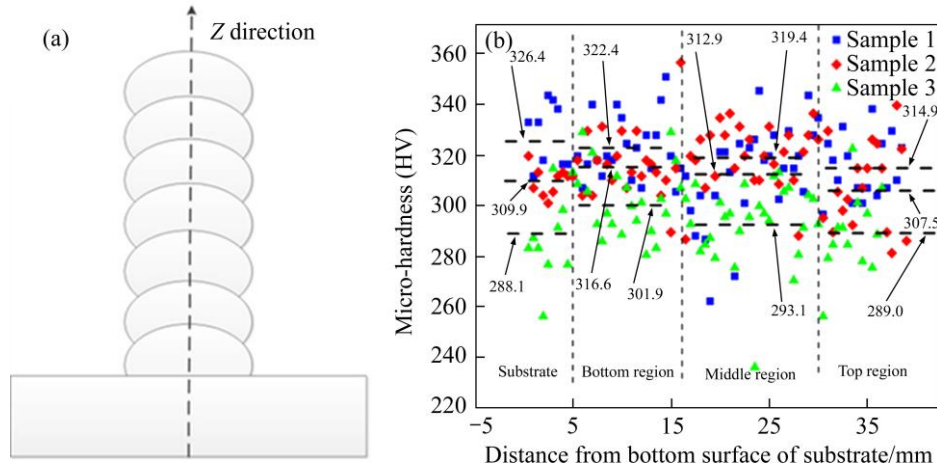


**Figure 8** Micro-hardness of WAALM Ti-6Al-4V components (Z direction)

top region. Although the data were rather scattered, the data were shown in Figure 8(b) can still show a slight trend of decrease in hardness from samples 1 to 3. That is, with the increase of deposition rate, the overall hardness decreases statistically. This probably can be attributed to the softening effect brought by the excessive heat input due to the larger deposition rate. As calculated above, sample 3 had the smallest cooling rate so that an overall coarser microstructure would be expected. In addition, the sequential deposition during the WAAM process causes the material to be heat treated up to 4–5 times and consequently the  $\alpha$  lamella would be coarsened leading to a smaller hardness.

## 4 Conclusions

In this study, the influence of WAAM deposition rate on the microstructure and mechanical properties of Ti6Al4V was investigated experimentally. The WAAM deposited Ti6Al4V components showed similar microstructures regardless of the deposition rate because the cooling rates were in the range between 130 and 160 K/s which was already in the lower regime for titanium phase transformation. There was a clear trend that the micro-hardness and ultimate tensile strength decrease with the increase of deposition rate, but the elongation was still scattered due to a possible inconsistency in the build quality.

## Acknowledgement

Projects(52075317, 51905333) supported by the National Natural Science Foundation of China; Project(IEC\NSFC\181278) supported by the Royal Society through International Exchanges 2018 Cost Share (China) Scheme; Project(19YF1418100) supported by Shanghai Sailing Program, China; Projects(19511106400, 19511106402) supported by Shanghai Science and Technology Committee Innovation, China; Project(2018ZD002B) supported by Karamay Science and Technology Major project; Project(2019E0235) supported by Aid for Xinjiang Science and Technology, China; Project(19030501300) supported by Shanghai Local Colleges and Universities Capacity Building Special Plan, China

## Contributors

ZHANG Pei-lei designed the project. JIA Zhi-yuan, TIAN Ying-tao and YAN Hua carried out data processing, performed data analysis. YU Zhi-shui, WU Di and SHI Hai-chuan offered some valuable suggestions for the contents of the manuscript. WANG Fu-xin, LEI Wei-sheng and MA Song-yun offered the specimen, performed data analysis. All authors replied to reviewers' comments and revised the final version.

## Conflict of interest

ZHANG Pei-lei, JIA Zhi-yuan, YAN Hua, YU Zhi-shui, WU Di, SHI Hai-chuan, WANG Fu-xin, TIAN Ying-tao, MA Song-yun and LEI Wei-sheng declare that they have no conflict of interest.

---

## References

- [1] CARROLL B E, PALMER T A, BEESE A M. Anisotropic tensile behavior of Ti–6Al–4V components fabricated with directed energy deposition additive manufacturing [J]. *Acta Mater*, 2015, 87: 309–320. DOI: <https://doi.org/10.1016/j.actamat.2014.12.054>.
- [2] DONACHIE M J. Titanium: A technical guide [M]. ASM International, 2000.
- [3] PETERS M, HEMPTENMACHER J, KUMPFERT J, LEYENS C. Structure and properties of titanium and titanium alloys [M]// *Titanium and Titanium Alloys: Fundamentals and Applications*. Weinheim, FRG: Wiley-VCH Verlag GmbH & Co., 2005: 1–36. DOI: <https://doi.org/10.1002/3527602119.ch1>.
- [4] LI Guo-jin, ZHANG Pei-lei, WU Xi, NIE Yun-peng, YU Zhi-shui, YAN Hua, LU Qing-hua. Gap bridging of 6061 aluminum alloy joints welded by variable-polarity cold metal transfer [J]. *Journal of Materials Processing Technology*, 2018, 255: 927–935. DOI: [10.1016/j.jmatprotec.2018.01.004](https://doi.org/10.1016/j.jmatprotec.2018.01.004).
- [5] NIE Y, ZHANG P, WU X, LI G, YAN H, YU Z. Rapid prototyping of 4043 Al-alloy parts by cold metal transfer [J]. *Science and Technology of Welding and Joining*, 2018, 23: 527–535. DOI: <https://doi.org/10.1080/13621718.2018.1438236>.
- [6] GU D D, MEINERS W, WISSENBACH K, POPRAWA R. Laser additive manufacturing of metallic components: Materials, processes and mechanisms [J]. *International Materials Reviews*, 2012, 57: 133–164. DOI: <https://doi.org/10.1179/1743280411Y.0000000014>.
- [7] HERZOG D, SEYDA V, WYCISK E, EMMELMANN C. Additive manufacturing of metals [J]. *Acta Mater*, 2016, 117: 371–392. DOI: <https://doi.org/10.1016/j.actamat.2016.07.019>.
- [8] MURR L E, MARTINEZ E, AMATO K N, GAYTAN S M, HERNANDEZ J, RAMIREZ D A, SHINDO P W, MEDINA F, WICKER R B. Fabrication of metal and alloy components by additive manufacturing: Examples of 3D materials science [J]. *Journal of Materials Research and Technology*, 2012, 1: 42–54. DOI: [https://doi.org/10.1016/S2238-7854\(12\)70009-1](https://doi.org/10.1016/S2238-7854(12)70009-1).
- [9] ZHANG Qi, ZHANG Pei-lei, YU Zhi-shui, YAN Hua, SHI Hai-chuan, WU Di, LI Shao-wei, TIAN Ying-tao. Microstructure and properties of an Al 6061/Galvanized plate fabricated by CMT welding [J]. *Journal of Wuhan University of Technology-Mater Sci Ed*, 2020, 35: 937–945. DOI: <https://doi.org/10.1007/s11595-020-2340-3>.
- [10] JIANG Q, ZHANG P L, YU Z S, SHI H C, LI S W, WU D, YAN H, YE X, CHEN J S. Microstructure and mechanical properties of thick-walled Inconel 625 alloy manufactured by WAAM with different torch paths [J]. *Advanced Engineering Materials*, 2021, 26(1): 2000728. DOI: <https://doi.org/10.1002/adem.202000728>.
- [11] LIU Zhi-qiang, ZHANG Pei-lei, LI Shao-wei, WU Di, YU Zhi-shui. Wire and arc additive manufacturing of 4043 Al alloy using a cold metal transfer method [J]. *International Journal of Minerals, Metallurgy and Materials*, 2020, 27: 783–791. DOI: <https://doi.org/10.1007/s12613-019-1930-6>.
- [12] WILLIAMS S W, MARTINA F, ADDISON A C, DING J, PARDAL G, COLEGROVE P. Wire+Arc additive manufacturing [J]. *Materials Science and Technology*, 2016, 32: 641–647. DOI: <https://doi.org/10.1179/1743284715Y.0000000073>.
- [13] RODRIGUES T A, DUARTE V, MIRANDA R M, SANTOS T G, OLIVEIRA J P. Current status and perspectives on wire and arc additive manufacturing (WAAM) [J]. *Materials*, 2019, 12: 1121. DOI: <https://doi.org/10.1179/1743284715Y.0000000073>.
- [14] CUNNINGHAM C R, FLYNN J M, SHOKRANI A, DHOKIA V, NEWMAN S T. Invited review article: Strategies and processes for high quality wire arc additive manufacturing [J]. *Additive Manufacturing*, 2018, 22: 672–686. DOI: <https://doi.org/10.1016/j.addma.2018.06.020>.
- [15] WU Bin-tao, PAN Zeng-xi, DING Dong-hong, CUIURI D, LI Hui-jun, XU Jing, NORRISH J. A review of the wire arc additive manufacturing of metals: properties, defects and quality improvement [J]. *Journal of Materials Processing Technology*, 2018, 35: 127–139. DOI: <https://doi.org/10.1016/J.JMAPRO.2018.08.001>.
- [16] LI Rui-di, WANG Min-bo, LI Zhi-ming, CAO Peng, YUAN Tie-chui, ZHU Hong-bin. Developing a high-strength Al-Mg-Si-Sc-Zr alloy for selective laser melting: Crack-inhibiting and multiple strengthening mechanisms [J]. *Acta Materialia*, 2020, 193: 83–98. DOI: <https://doi.org/10.1016/j.actamat.2020.03.060>.
- [17] ALMEIDA P, WILLIAMS S. Innovative process model of Ti–6Al–4V additive layer manufacturing using cold metal transfer (CMT) [C]// *Proceedings of the 21st Annual International Solid Freeform Fabrication Symposium*. Austin, Texas, 2010: 25–36.
- [18] KIM B, RITZDORF T. Electrical waveform mediated through-mask deposition of solder bumps for wafer level packaging [J]. *Journal of The Electrochemical Society*, 2004, 151: C342. DOI: <https://doi.org/10.1149/1.1690784>.
- [19] WANG F, WILLIAMS S, COLEGROVE P, ANTONYSAMY A A. Microstructure and mechanical properties of wire and arc additive manufactured Ti-6Al-4V [J] *Metallurgical and Materials Transactions A*, 2013, 44: 968–977. DOI: <https://doi.org/10.1007/s11661-012-1444-6>.
- [20] ZHOU J, TSAI H L. Developments in pulsed and continuous wave laser welding technologies [M]// *Handbook of Laser Welding Technologies*. Amsterdam: Elsevier, 2013: 103–148e. DOI: <https://doi.org/10.1533/9780857098771.1.103>.
- [21] MARTINA F, MEHNEN J, WILLIAMS S W, COLEGROVE P, WANG F. Investigation of the benefits of plasma deposition for the additive layer manufacture of Ti–6Al–4V [J]. *Journal of Materials Processing Technology*, 2012, 212: 1377–1386. DOI: <https://doi.org/10.1016/J.JMATPROTEC.2012.02.002>.
- [22] BAUFELD B, van der BIEST O, GAULT R. Microstructure of Ti-6Al-4V specimens produced by shaped metal deposition [J]. *International Journal of Materials Research*, 2009, 100(11): 1536–1542. DOI: <https://doi.org/10.3139/146.110217>.
- [23] CHENG Jiang-bo, FENG Yuan, YAN Chen, HU Xian-long, LI Rui-feng, LIANG Xiu-bing. Development and characterization of Al-

- Based amorphous coating [J]. *JOM*, 2020, 72: 745–753. DOI: <https://doi.org/10.1007/s11837-019-03966-y>.
- [24] HO A, ZHAO H, FELLOWES J W, MARTINA F, DAVIS A E, PRANGNELL P B. On the origin of microstructural banding in Ti-6Al4V wire-arc based high deposition rate additive manufacturing [J]. *Acta Materialia*, 2019, 166: 306–323. DOI: <https://doi.org/10.1016/j.actamat.2018.12.038>.
- [25] FRAZIER W E. Metal additive manufacturing: A review [J]. *Journal of Materials Engineering and Performance*, 2014, 23: 1917–1928. DOI: <https://doi.org/10.1007/s11665-014-0958-z>.
- [26] MARTINA F, ROY M J, SZOST B A, TERZI S, COLEGROVE P A, WILLIAMS S W, WITHERS P J, MEYER J, HOFMANN M. Residual stress of as-deposited and rolled wire+arc additive manufacturing Ti-6Al-4V components [J]. *Materials Science and Technology*, 2016, 32: 1439–1448. DOI: <https://doi.org/10.1080/02670836.2016.1142704>.
- [27] MCANDREW A R, ALVAREZ ROSALES M, COLEGROVE P A, HÖNNIGE J R, HO A, FAYOLLE R, EYITAYO K, STAN I, SUKRONGPANG P, et al. Interpass rolling of Ti-6Al-4V wire + arc additively manufactured features for microstructural refinement [J]. *Additive Manufacturing*, 2018, 21: 340–349. DOI: <https://doi.org/10.1016/J.ADDMA.2018.03.006>.
- [28] DONOGHUE J, ANTONYSAMY A A, MARTINA F, COLEGROVE P A, WILLIAMS S W, PRANGNELL P B. The effectiveness of combining rolling deformation with wire-arc additive manufacture on  $\beta$ -grain refinement and texture modification in Ti-6Al-4V [J]. *Materials Characterization*, 2016, 114: 103–114. DOI: <https://doi.org/10.1016/j.matchar.2016.02.001>.
- [29] HÖNNIGE J R, COLEGROVE P A, AHMAD B, FITZPATRICK M E, GANGULY S, LEE T L, WILLIAMS S W. Residual stress and texture control in Ti-6Al-4V wire + arc additively manufactured intersections by stress relief and rolling [J]. *Materials & Design*, 2018, 150: 193–205. DOI: <https://doi.org/10.1016/J.MATDES.2018.03.065>.
- [30] WU Bin-tao, PAN Zeng-xi, DING Dong-hong, CUIURI D, LI Hui-jun, FEI Zhen-yu. The effects of forced interpass cooling on the material properties of wire arc additively manufactured Ti6Al4V alloy [J]. *Journal of Materials Processing Technology*, 2018, 258: 97–105. DOI: <https://doi.org/10.1016/j.jmatprotec.2018.03.024>.
- [31] BAUFELD B, BRANDL E, van der BIEST O. Wire based additive layer manufacturing: Comparison of microstructure and mechanical properties of Ti-6Al-4V components fabricated by laser-beam deposition and shaped metal deposition [J]. *Journal of Materials Processing Technology*, 2011, 211: 1146–1158. DOI: <https://doi.org/10.1016/j.jmatprotec.2011.01.018>.
- [32] BAUFELD B. Effect of deposition parameters on mechanical properties of shaped metal deposition parts [J]. *Proceedings of the Institution of Mechanical Engineers, Part B: Journal of Engineering Manufacture*, 2012, 226: 126–136. DOI: <https://doi.org/10.1177/0954405411403669>.
- [33] BERMINGHAM M J, NICASTRO L, KENT D, CHEN Y, DARGUSCH M S. Optimising the mechanical properties of Ti-6Al-4V components produced by wire + arc additive manufacturing with post-process heat treatments [J]. *Journal of Alloys and Compounds*, 2018, 753: 247–255. DOI: <https://doi.org/10.1016/J.JALLCOM.2018.04.158>.
- [34] QIAN Gui-an, JIAN Zhi-mo, QIAN Yu-jia, PAN Xiang-nan, MA Xian-feng, HONG You-shi. Very-high-cycle fatigue behavior of AlSi10Mg manufactured by selective laser melting: Effect of build orientation and mean stress [J]. *Int J Fatigue*, 2020, 138: 105696. DOI: <https://doi.org/10.1016/j.ijfatigue.2020.105696>.
- [35] QIAN Gui-an, LI Yan-feng, PAOLINO D S, TRIDELLO A, BERTO F, HONG You-shi. Very-high-cycle fatigue behavior of Ti-6Al-4V manufactured by selective laser melting: Effect of build orientation [J]. *International Journal of Fatigue*, 2020, 136: 105628. DOI: <https://doi.org/10.1016/j.ijfatigue.2020.105628>.
- [36] WU Bin-tao, PAN Zeng-xi, DING Dong-hong, CUIURI D, LI Hui-jun. Effects of heat accumulation on microstructure and mechanical properties of Ti6Al4V alloy deposited by wire arc additive manufacturing [J]. *Additive Manufacturing*, 2018, 23: 151–160. DOI: <https://doi.org/10.1016/j.addma.2018.08.004>.
- [37] TIAN Yin-bao, SHEN Jun-qi, HU Sheng-sun, GOU Jian, CUI Yan. Effects of cold metal transfer mode on the reaction layer of wire and arc additive-manufactured Ti-6Al-4V/Al-6.25Cu dissimilar alloys [J]. *Journal of Materials Science & Technology*, 2021, 74: 35–45. DOI: <https://doi.org/10.1016/j.jmst.2020.09.014>.
- [38] GOU Jian, SHEN Jun-qi, HU Sheng-sun, TIAN Yin-bao, LIANG Ying. Microstructure and mechanical properties of as-built and heat-treated Ti-6Al-4V alloy prepared by cold metal transfer additive manufacturing [J]. *Journal of Manufacturing Processes*, 2019, 42: 41–50. DOI: <https://doi.org/10.1016/j.jmapro.2019.04.012>.
- [39] BAI Xing-wang, COLEGROVE P, DING Jia-luo, ZHOU Xiang-man, DIAO Cheng-lei, BRIDGEMAN P, ROMAN HÖNNIGE J, ZHANG Hai-ou, WILLIAMS S. Numerical analysis of heat transfer and fluid flow in multilayer deposition of PAW-based wire and arc additive manufacturing [J]. *International Journal of Heat and Mass Transfer*, 2018, 124: 504–516. DOI: <https://doi.org/10.1016/j.ijheatmasstransfer.2018.03.085>.
- [40] AHMED T, RACK H J. Phase transformations during cooling in  $\alpha+\beta$  titanium alloys [J]. *Materials Science and Engineering: A*, 1998, 243: 206–211. DOI: [https://doi.org/10.1016/S0921-5093\(97\)00802-2](https://doi.org/10.1016/S0921-5093(97)00802-2).
- [41] ROSENTHAL D. The theory of moving sources of heat and its application to metal treatments [J]. *Transactions ASME*, 1946, 43: 849–866.
- [42] DING Dong-hong, PAN Zeng-xi, CUIURI D, LI Hui-jun. Wire-feed additive manufacturing of metal components: technologies, developments and future interests [J]. *The International Journal of Advanced Manufacturing Technology*, 2015, 81: 465–481. DOI: <https://doi.org/10.1007/s00170-015-7077-3>.
- [43] ZHAO H, HO A, DAVIS A, ANTONYSAMY A, PRANGNELL P. Automated image mapping and quantification of microstructure heterogeneity in additive manufactured Ti6Al4V [J]. *Materials Characterization*, 2019, 147: 131–145. DOI: <https://doi.org/10.1016/J.MATCHAR.2018.10.027>.

- 
- [44] KOBRYN P, SEMLATIN S. Microstructure and texture evolution during solidification processing of Ti–6Al–4V [J]. *Journal of Materials Processing Technology*, 2003, 135: 330–339. DOI: [https://doi.org/10.1016/S0924-136\(02\)00865-8](https://doi.org/10.1016/S0924-136(02)00865-8).
- [45] SING S L, AN J, YEONG W Y, WIRIA F E. Laser and electron-beam powder-bed additive manufacturing of metallic implants: A review on processes, materials and designs [J]. *Journal of Orthopaedic Research*, 2016, 34: 369–385. DOI: <https://doi.org/10.1002/jor.23075>.
- [46] WARMUTH F, OSMANLIC F, ADLER L, LODES M A, KÖRNER C. Fabrication and characterisation of a fully auxetic 3D lattice structure via selective electron beam melting [J]. *Smart Materials and Structures*, 2017, 26(2): 025013. DOI: <https://doi.org/10.1088/1361-65X/26/2/025013>.